

# An exact quantification of backreaction in relativistic cosmology

Timothy Clifton,<sup>1,2</sup> Kjell Rosquist,<sup>3,4</sup> and Reza Tavakol<sup>2</sup>

<sup>1</sup>*Department of Astrophysics, University of Oxford, UK.*

<sup>2</sup>*School of Physics and Astronomy, Queen Mary University of London, Mile End Road, London E1 4NS, UK.*

<sup>3</sup>*Department of Physics, Stockholm University, 106 91 Stockholm, Sweden.*

<sup>4</sup>*ICRANet, Piazza della Repubblica, 10 I-65122 Pescara, Italy*

An important open question in cosmology is the degree to which the Friedmann-Lemaître-Robertson-Walker (FLRW) solutions of Einstein’s equations are able to model the large-scale behaviour of the locally inhomogeneous observable universe. We investigate this problem by considering a range of *exact*  $n$ -body solutions of Einstein’s constraint equations. These solutions contain discrete masses, and so allow arbitrarily large density contrasts to be modelled. We restrict our study to regularly arranged distributions of masses in topological 3-spheres. This has the benefit of allowing straightforward comparisons to be made with FLRW solutions, as both spacetimes admit a discrete group of symmetries. It also provides a time-symmetric hypersurface at the moment of maximum expansion that allows the constraint equations to be solved exactly. We find that when all the mass in the universe is condensed into a small number of objects ( $\lesssim 10$ ) then the amount of backreaction in dust models can be large, with  $O(1)$  deviations from the predictions of the corresponding FLRW solutions. When the number of masses is large ( $\gtrsim 100$ ), however, then our measures of backreaction become small ( $\lesssim 1\%$ ). This result does not rely on any averaging procedures, which are notoriously hard to define uniquely in general relativity, and so provides (to the best of our knowledge) the first exact and unambiguous demonstration of backreaction in general relativistic cosmological modelling. Discrete models such as these can therefore be used as laboratories to test ideas about backreaction that could be applied in more complicated and realistic settings.

PACS numbers: 98.80.Jk, 04.20.Jb

## I. INTRODUCTION

The visible matter in the universe contains structure on a wide range of scales, from stars and planets ( $\sim 10^{10}\text{m}$ ) to voids and super-clusters ( $\sim 10^{24}\text{m}$ ), (see e.g. [1]). In standard general relativistic cosmological modelling the problem of dealing with this complexity is often circumvented by assuming that the stress-energy tensor of an inhomogeneous universe can be approximated by an ‘averaged’ stress-energy tensor, usually assumed to be representable by a simple perfect fluid, while leaving the left hand side of Einstein’s equations unchanged. The solution to these equations is then taken to represent the geometry of spacetime on the scale over which the averaging was performed. If this scale is large enough to result in a homogeneous and isotropic spacetime, then we will refer to this geometry as the “background”.

The great benefit of this approach is the enormous simplification it entails, by allowing cosmology to be done on any scale, without having to worry about the enormously complicated task of taking into account the wide range of structures that exist in the universe. The drawback is that it is not always clear to what extent the expansion of space in the background geometry is representative of the large-scale expansion of space in the actual universe. For a given model, we will refer to the difference between these two things as “backreaction”, which can be considered as the influence of inhomogeneities at different scales on large-scale cosmological dynamics. As large-scale expansion can be related to observables such as luminosity distance and redshift [2–4], it is therefore the case that

an understanding of backreaction could prove essential in achieving a fundamental concordance between theory and observations [5, 6].

This task becomes increasingly important given that observational cosmology is now starting to be able to make high-precision measurements of a variety of different astrophysical probes, including the Cosmic Microwave Background (CMB) [7, 8], Type Ia supernovae [9, 10], and Baryon Acoustic Oscillations (BAO) [11, 12]. When interpreted within the background of the standard cosmological model, these very different probes all suggest that the universe is at present undergoing a phase of late-time accelerated expansion. In a genuinely homogeneous and isotropic general relativistic universe filled with a perfect fluid, such behaviour is only possible if  $p < -\rho/3$ , with data currently being compatible with the presence of a cosmological constant with  $p = -\rho$ . The presence of such a fluid is problematic for a variety of reasons, requiring a fine-tuning of perhaps as much as 1 part in  $10^{120}$ . This immediately raises the question of whether the model we are using to interpret the data is adequate, a question which needs to be quantified in any case if we are to start performing “precision cosmology” [13].

One particular aspect of this complicated problem is the degree to which dust (a fluid without any self-interactions) is appropriate for describing the matter content of the universe [14]. This approximation treats gravitationally bound, extended objects (such as galaxies, and clusters of galaxies) as a medium that is parametrised by only a handful of continuous, and usually slowly varying, quantities. Within this framework, the spacetime

through which photons travel has a fundamentally different type of curvature to that of the real universe [15]. It also ignores the gravitational consequences of the binding energies between and within astrophysical systems [16]. A dust description should therefore be considered as an approximation only, and must itself be investigated in order to ascertain the extent to which it is justifiable.

We study the problems outlined above by considering cosmological solutions that are explicitly composed of regularly arranged discrete masses. These solutions consist of vacuum everywhere exterior to the sources under consideration, and are constructed on a manifold that has spacelike hypersurfaces that are topological 3-spheres. As a result, they admit a group of discrete symmetries corresponding to rotations of the 3-sphere that leave the positions of the masses invariant. These models are among the simplest possible inhomogeneous spacetimes that could be considered to exhibit large-scale homogeneity and isotropy: They introduce only one extra scale into the problem (the inter-particle separation), they are vacuum solutions of the field equations (up to the singularities), and they contain within them a time-symmetric spatial hypersurface (which greatly simplifies the constraint equations). This makes them ideal candidates for studying backreaction.

Cosmological solutions of this type have been considered before, starting with the seminal work of Lindquist and Wheeler [17]. The approach these authors took was to construct a gravitational analogue of the highly successful Wigner-Seitz construction. The basic idea was to build lattices from regular cells, and attach the cell boundaries tangentially to a background 3-sphere. Dynamics were then imposed by assuming that observers that are equidistant between neighbouring sources should be falling freely with respect to those sources. This led to a dynamical model of the universe in which the masses are regularly arranged, and that is taken to be an approximate solution to Einstein's equations. The Lindquist-Wheeler approach has recently been extended to include models with spatially flat and open topologies [18], as well as to models with a cosmological constant [19]. The optical properties of spatially flat models of this type have also been considered in [18–20], as have those of negatively curved models in [21]. Other attempts to construct cosmological models for similar configurations of discrete masses have been made using perturbative expansions [22], and Regge calculus [23].

While providing insights into the problem, all of the models mentioned above involve the use of approximate solutions. Our aim here is to take an alternative approach to addressing this problem that is exact. This approach is based on work initiated by Misner about five decades ago [24], and that has subsequently been used extensively in the study of black hole physics [25–27]. The underlying idea here is again drawn from analogy with the study of electromagnetism, where intuitions about more general situations are gained by first studying the simple case of static configurations of charge. In gravitational settings,

however, it is very difficult to arrange for configurations of isolated masses to be static for a finite interval of time<sup>1</sup>. In contrast, configurations that are *instantaneously* static occur frequently. The study of such configurations, that occur in many systems of physical interest, is referred to as geometrostatics<sup>2</sup>.

In the case of cosmology, which is our main interest here, an important example is provided by the instantaneously static (and therefore time-symmetric) hypersurfaces that occur at the moment of maximum expansion in dust-dominated FLRW solutions with positive spatial curvature. Our goal is to construct a set of instantaneously static configurations that are exact, and that contain discrete matter sources, rather than continuous fluids. We do this by constructing regular tessellations of a 3-sphere by using different sets of identical polyhedra, each with an identical mass at their centre. We show that the method of geometrostatics can be extended to solve the constraint equations *exactly* in these cases. Our aim is then to use these solutions to study backreaction in dust filled cosmological models. We do this by comparing the time-symmetric spatial hypersurfaces of the exact discrete solutions to the corresponding FLRW solutions with the same proper mass<sup>3</sup>, and considering, in particular, the extent to which the FLRW solutions emerge as the number of sources is increased. This provides a *precise* indication of the degree to which FLRW solutions can be used to represent initial configurations for spacetimes that contain discrete objects. A fuller investigation of backreaction along these lines would also include considering the dynamical evolution of models with discrete sources. We leave this for a future publication.

The plan of the paper is as follows. In Section II we recap on perfect fluid FLRW cosmology. In Section III we provide the constraint equations on time-symmetric hypersurfaces for discrete masses on a 3-sphere. We discuss the Schwarzschild solution, and then outline how to find the solution for arbitrarily many discrete masses in a closed space. In Section IV we construct all of the possible solutions that consist of discrete sources regularly arranged on a closed lattice. This allows us to explain why there are no 2-mass solutions with spherical topology to Einstein's equations that admit a time-symmetric hypersurface. In Section V we provide evidence that shows that the sources in our discrete models are always separated by distances that are larger than their horizon sizes at the maximum of expansion. In Section VI we investigate backreaction in dust-dominated cosmological

<sup>1</sup> Counter-examples include spacetimes in which the cosmological constant is non-zero, and the periodic solution found by Korotkin and Nicolai [28].

<sup>2</sup> Examples include dynamical systems that possess a recollapsing phase (as happens when a particle is thrown vertically upwards from the surface of a massive body, with less than the escape velocity).

<sup>3</sup> As defined in [29] and in Section III B.

models by comparing the scale of our lattices to dust-filled FLRW solutions of Einstein's equations with the same total proper mass. We find that  $O(1)$  deviations from the results of Friedmann cosmology can occur when the number of masses is small ( $\lesssim 10$ ), but that the scale of the solutions converge to the Friedmann values when there are very many masses ( $\gtrsim 100$ ). In Section VII we then consider what happens when we include inter-particle interaction energies in our definition of mass. We find that the consequences of changing the number of masses in the lattice, while keeping the total energy of the system the same, can considerably change the scale of the hypersurface of maximum expansion. This shows that although backreaction in dust models we consider is generically quite small, the consequences of ignoring interaction energies when using the dust approximation can hide potentially interesting effects. In Section VIII we present our conclusions.

## II. PERFECT FLUID COSMOLOGY

The spatially homogeneous and isotropic perfect fluid FLRW solutions have a geometry given by

$$ds^2 = -f(t)dt^2 + a^2(t) (d\chi^2 + h^2(\chi)d\Omega^2), \quad (1)$$

where  $f(t)$  is a free function,  $d\Omega^2 = d\theta^2 + \sin^2(\theta)d\phi^2$ , and  $h(\chi) = \sin \chi$ ,  $\chi$  or  $\sinh \chi$  for solutions with spatial curvature  $k = +1, 0$  or  $-1$ , respectively. The scale factor  $a(t)$  satisfies the constraint equation

$$\frac{1}{f} \frac{\dot{a}^2}{a^2} = \frac{8\pi}{3} \rho - \frac{k}{a^2}, \quad (2)$$

where the dot represents a derivative with respect to  $t$ , and  $\rho = \rho(t)$  is the energy density of the continuous perfect fluid, which obeys the conservation equation

$$\dot{\rho} + 3\frac{\dot{a}}{a}(\rho + p) = 0, \quad (3)$$

where  $p = p(t)$  is the pressure. This completely specifies the solution, up to constants of integration.

For the present study we will be primarily interested in models with positive spatial curvature ( $k = +1$ ), and with a pressureless dust source ( $p = 0$ ). In this case, if we take  $f = a(t)$ , then the solution can be written as

$$a(t) = \frac{8\pi}{3} \rho_0 - \frac{1}{4}(t - t_0)^2, \quad (4)$$

where  $t_0$  and  $\rho_0$  are constants, and where  $\rho(t) = \rho_0/a^3(t)$ . The maximum of expansion can then be seen to occur at  $t = t_0$ , and the geometry of the hypersurface  $t = t_0$  can be seen to be given by

$$dl^2 = \frac{3}{8\pi\rho(t_0)} (d\chi^2 + \sin^2\chi d\Omega^2), \quad (5)$$

which is rigidly specified once  $\rho(t_0)$ , the energy density at maximum of expansion, is known.

We note that the only dust-filled FLRW solutions that admit a time-symmetric hypersurface are spatially closed, with a spherical topology. Interestingly, the boundary conditions for discrete models with a momentarily static distribution of sources also seem to be incompatible with open topologies (the reason for this is that a  $1/r$  source cannot live alone on  $T^3$ , and a regular lattice of identical sources on  $E^3$  is also not possible [28]). This shows a certain qualitative concordance between discrete and fluid solutions in the interplay between boundary conditions and topology.

## III. CONSTRAINT EQUATIONS FOR DISCRETE MODELS

Our aim here is to obtain exact vacuum solutions of Einstein's equations corresponding to regular lattices of sources that are instantaneously at rest on a topological 3-sphere.

In such a setting the relevant equations to solve are the Gauss-Codazzi equations:

$$\mathcal{R} + K^2 - K_{ij}K^{ij} = 0 \quad (6)$$

$$(K_i^j - \delta_i^j K)_{|j} = 0, \quad (7)$$

where  $\mathcal{R}$  is the Ricci curvature of the 3-space,  $K_{ij}$  is the extrinsic curvature of the 3-space in the 4-dimensional spacetime, and  $K = K_i^i$ . The indices  $i, j$  refer to coordinates in the 3-space, and the vertical line denotes covariant derivative in that space.

It is well known that if we choose a time coordinate that is specified by the normal derivative to this initial hypersurface (such that  $g_{t\mu} = -\delta_\mu^t$ ), then the extrinsic curvature can be written as  $K_{ij} = -\frac{1}{2}g_{ij,t}$ . Instantaneously static hypersurfaces therefore have  $K_{ij} = 0$ , and the Gauss-Codazzi equations reduce simply to

$$\mathcal{R} = 0. \quad (8)$$

A key point here is that for any 3-dimensional geometry that satisfies the initial constraint (8) there is a unique 4-dimensional spacetime that satisfies the full Einstein equations. This is the method of geometrostatics, presented by Misner in [24], and studied for the case of asymptotically flat space in [25–27].

Here we are interested in solving Eq. (8) in closed spaces. In this case we can make the following ansatz for the metric of the spatial 3-section

$$dl^2 = \psi^4 \hat{h}_{ij} dx^i dx^j, \quad (9)$$

where  $\psi = \psi(x^i)$ , and where  $\hat{h}_{ij}$  is the metric of a 3-sphere with constant curvature  $\hat{\mathcal{R}}$ . The Gauss-Codazzi equations are then satisfied if  $\psi$  obeys the Helmholtz

equation:

$$\hat{\nabla}^2 \psi = \frac{1}{8} \hat{\mathcal{R}} \psi, \quad (10)$$

where  $\hat{\nabla}^2$  is the Laplacian corresponding to  $\hat{h}_{ij}$ .

### A. A Single Schwarzschild Mass

The Schwarzschild solution has been well studied using asymptotically flat solutions in geometrostatics, including in the original work of Misner [24]. It is important to note that the Schwarzschild solution is still a solution in the present case, as the 3-sphere is conformally flat. In this case, however, there will be a different radial variable and a different functional form for the conformal factor  $\psi$ . Given the linearity of the Helmholtz equation, (10), it can be seen that multi-source solutions can be constructed by linear superposition of the solutions for single sources.

In asymptotically flat, isotropic coordinates, a static spacelike slice of the Schwarzschild solution can be written as

$$dl^2 = \left(1 + \frac{m}{2\tilde{r}}\right)^4 (d\tilde{r}^2 + \tilde{r}^2 d\Omega^2), \quad (11)$$

where  $m$  is a constant. Performing the coordinate transformation  $\tilde{r} = K \tan \frac{\chi}{2}$ , where  $K$  is a constant, it can be seen that Eq. (11) becomes

$$dl^2 = \frac{K^2}{4} \left[ \frac{1}{\cos \frac{\chi}{2}} + \frac{m}{2K \sin \frac{\chi}{2}} \right]^4 (d\chi^2 + \sin^2 \chi d\Omega^2). \quad (12)$$

This metric is clearly of the same form as Eq. (9), and solves Eq. (10), with  $\hat{\mathcal{R}} = 6$  (for a unit 3-sphere) and

$$\psi = \sqrt{\frac{K}{2}} \left( \frac{1}{\cos \frac{\chi}{2}} + \frac{m}{2K \sin \frac{\chi}{2}} \right). \quad (13)$$

Actually, both functions  $A(\chi) := (\sin \frac{\chi}{2})^{-1}$  and  $B(\chi) := (\cos \frac{\chi}{2})^{-1}$  satisfy Eq. (8) with  $\hat{\mathcal{R}} = 6$ .

This means that although the term in Eq. (12) that corresponds directly to the  $2m/r$  source term from Eq. (11) can be seen to be the one that is proportional to  $A(\chi)$ , the term that is proportional to  $B(\chi)$  can also be treated as a source, although it is located at the antipode. This becomes obvious if we place the origin of the spherical coordinates at the antipode by the transformation  $\chi \rightarrow \pi - \chi$ , as in that case the roles of the two terms in Eq. (12) are interchanged (i.e.  $A(\chi) \rightarrow B(\chi)$  and  $B(\chi) \rightarrow A(\chi)$ ). Thus it appears that placing a Schwarzschild source on the 3-sphere induces a mirror source at the antipode. Furthermore, these two source terms are joined at their horizons, as is clear if we set the gauge parameter to  $K = m/2$  (in which case the horizon at  $\tilde{r} = m/2$  appears at  $\chi = \pi/2$  in the hyperspherical coordinates).

One can then consider that as  $\chi \rightarrow \pi$  one approaches either the asymptotic region where  $\tilde{r} \rightarrow \infty$ , or that one approaches another Schwarzschild mass. These two situations are geometrically identical, and there is therefore no difference between the one mass solutions and the two mass solution (as long as the point at  $\chi = \pi$  can be added to the manifold).

### B. Many Schwarzschild Masses

From Eq. (12) we can now infer that there exist multi-source solutions on the 3-sphere that take the form

$$dl^2 = \psi^4 (d\chi^2 + \sin^2 \chi d\Omega^2), \quad (14)$$

where  $\psi = \psi(\chi, \theta, \phi)$  is given by

$$\psi(\chi, \theta, \phi) = \sum_{i=1}^N \frac{\sqrt{\tilde{m}_i}}{2f_i(\chi, \theta, \phi)}, \quad (15)$$

where the mass parameters  $\tilde{m}_i$  are a set of constants and  $f_i(\chi, \theta, \phi) = \sin(\chi_i/2)$ . Here the  $\chi_i$  refer to new coordinates  $(\chi_i, \theta_i, \phi_i)$  which are obtained by rotating the coordinates  $(\chi, \theta, \phi)$  in Eq. (14) so that the  $i$ 'th source position appears at  $\chi_i = 0$ .

It follows from the form of Eq. (14) that one cannot adjust the  $\tilde{m}_i$  and the size of the 3-sphere independently. For example, scaling the size of the 3-sphere by a constant  $\alpha^2$  automatically results in scaling the  $\tilde{m}_i$  by a factor  $\alpha$ . This demonstrates that there exists a certain rigidity in the configuration, once the  $\tilde{m}_i$  are specified. Specifying the value of the  $\tilde{m}_i$  is therefore crucial for determining any measure of distance in our hypersurface. Once they are specified, however, then all measures of distance can be calculated uniquely.

When considering the original single source Schwarzschild solution, the parameters  $\tilde{m}_i$  ( $\tilde{m}_1$  and  $\tilde{m}_2$  in that case) are equal to the standard Schwarzschild mass,  $\tilde{m}_1 = \tilde{m}_2 = m$  (using the gauge  $K = m/2$ ). However, when multiple sources are present, the interpretation of the  $\tilde{m}_i$  parameters will instead be that of an *effective mass* which includes the binding energies with respect to all the other objects in the universe (cf. [25]). However, their actual, locally measured, *proper mass*<sup>4</sup> must be determined by the requirement

<sup>4</sup> This term is used in analogy with the proper mass defined by Wald [29, p.126]. In the context of asymptotically flat spacetimes, Brill and Lindquist [25] use the term *bare mass*, as it is used in particle physics. We prefer not to use this term here since the situations in cosmology and particle physics are opposites with respect to how masses are measured. In particle physics, the observer is outside the system and cannot measure the bare mass directly. In cosmology, on the other hand, the observer is inside the system and therefore measures the bare mass (in particle physics terminology).

that the geometry reduces to that given by Eq. (12) in the limit  $\chi \rightarrow 0$ , in analogy with the asymptotically flat situation analysed in Ref. [25]. It can be shown that the proper mass defined in this way is equivalent to the mass in the Schwarzschild region at the other end of the Einstein-Rosen bridge of the black hole.

To summarise, these two mass definitions are:

- 1 *The Effective Mass*,  $(m_i)_{\text{eff}}$ , is defined to be equal to the mass parameter of the corresponding source,  $(m_i)_{\text{eff}} := \tilde{m}_i$ .
- 2 *The Proper Mass*,  $m_i$ , is defined in such a way that the geometry of the space in the vicinity of each object is given by Eq. (12), in the limit  $\chi \rightarrow 0$ .

Strictly speaking, one requires a region to exist that is infinitely far away from all of the masses in order to have an operational definition of the gravitational effect of the inter-particle potentials that are included in the effective mass. This is clearly impossible in the case of a closed space, but this does not stop us from drawing an analogy with cases in which asymptotically distant regions do exist.

#### IV. LATTICE SOLUTIONS

Using the above ingredients we can now construct a set of models with different numbers of regularly arranged discrete masses on a 3-sphere. To do this we proceed in analogy with the approach taken by Lindquist and Wheeler [17], so that our models are constructed by considering all of the possible regular tessellations of the 3-sphere. We then place identical masses at the centre of each cell, with the result that the distribution of masses is such that the distance between any mass and its nearest neighbours is the same for each of them.

There are six possible regular tessellations of the 3-sphere, those with 5, 8, 16, 24, 120 and 600 polyhedra [30]. In addition, one can also cover a hypersphere with 2 balls [31]. These possibilities are displayed in Table I. Using these tessellations, we will now proceed to construct a sequence of exact discrete regular lattice models of the universe, with increasing numbers of sources, on a time-symmetric 3-sphere. Our discrete models will consist of  $n$  equal masses (where  $n = 2, 5, 8, 16, 24, 120, 600$ ). By positioning these masses at the centre of each of the cells, they are at a maximum possible distance away from each of their neighbours.

##### A. The 2-Cell model

The 2-cell model, consisting of two balls with their boundaries identified, is the exceptional case of the structures listed in Table I. Its cells are not regular polyhedra (and hence it has no Schläfli symbol), and it was not considered in either [17] or [30]. Nevertheless, a lattice with

Lattice Structure	Cell Shape	Number of Cells
-	Ball	2
{333}	Tetrahedron	5
{433}	Cube	8
{334}	Tetrahedron	16
{343}	Octahedron	24
{533}	Dodecahedron	120
{335}	Tetrahedron	600

Table I: All possible regular tessellations of the 3-sphere. The ‘Lattice Structure’ is given by the Schläfli symbols  $\{pqr\}$ , where  $p$  is the number of edges to a face,  $q$  is the number of faces that meet at a vertex, and  $r$  are the number of cells that meet at an edge [30].

2 cells seems like a perfectly legitimate object to consider<sup>5</sup> and has indeed been studied recently in [31]. The authors of this paper found that the geometry inside each cell could only be matched at the junction between cells if that junction was a horizon. They also found that no solutions exist unless the cosmological constant  $\Lambda \neq 0$ .

Let us now consider this 2-cell model using the initial value formalism discussed above. The source functions in this case are given by  $f_1 = \sin(\chi/2)$  and  $f_2 = \cos(\chi/2)$ , with  $\tilde{m}_1 = \tilde{m}_2 = m$ . Substituting into Eq. (14) then gives

$$\psi = \frac{\sqrt{m}}{2 \cos \frac{\chi}{2}} + \frac{\sqrt{m}}{2 \sin \frac{\chi}{2}}, \quad (16)$$

which is clearly just the Schwarzschild solution given in Eq. (12), with  $K = m/2$ . As explained above, this model can be considered to consist of two sources centred at opposite poles and matched (analytically continued in fact) across their horizons. Within this interpretation the exterior parts of the sources are missing, and there are consequently no static regions outside of the black holes. Because of the absence of an exterior region between the sources, the 2-cell model is unsuitable for cosmology. This result provides an alternate illustration of the findings in Ref. [31].

##### B. The 5-Cell model

Let us now consider the 5-cell model (or *hyperpyramid*), that consists of 5 tetrahedra. This structure, which is in fact a 4-simplex, is the tessellation in Table I with the fewest number of cells that are regular polyhedra. To obtain the coordinates of the masses at the centres of the

<sup>5</sup> This object does, in fact, have a considerable advantage over the lattices in Table I, as the geometry around each mass must be spherically symmetric, and so is considerably easier to solve for. This means that the approximations used by Lindquist and Wheeler in [17] are not required in this case at all.

tetrahedra one can consider a hyperpyramid in the embedding space  $E^4$ , and place a unit 3-sphere inside the hyperpyramid such that the two structures touch at the centre of each of the 5 tetrahedral cells. Alternatively, one could consider the positions of the vertices of the dual lattice<sup>6</sup>, which in this case is another hyperpyramid. The coordinates of the 5 masses that result are given in the Table II, below.

To define the model we use spherical polar coordinates which are related to Cartesian coordinates of  $E^4$  by

$$\begin{aligned} w &= \cos \chi \\ x &= \sin \chi \cos \theta \\ y &= \sin \chi \sin \theta \cos \phi \\ z &= \sin \chi \sin \theta \sin \phi. \end{aligned} \quad (17)$$

The source functions,  $f_i$ , from Eq. (14), are then

$$f_i = \sin \left[ \frac{1}{2} \cos^{-1}(h_i) \right], \quad (18)$$

where the functions,  $h_i$ , defined in Eq. (18) are given by

$$\begin{aligned} h_1 &= \cos \chi \\ h_2 &= \frac{\sqrt{15}}{4} \cos \theta \sin \chi - \frac{\cos \chi}{4} \\ h_3 &= \sqrt{\frac{5}{6}} \sin \chi \sin \theta \cos \phi \\ &\quad - \sqrt{\frac{5}{48}} \sin \chi \cos \theta - \frac{\cos \chi}{4} \\ h_4 &= \sqrt{\frac{5}{6}} \sin \chi \sin \theta \sin \left( \phi - \frac{\pi}{6} \right) \\ &\quad - \sqrt{\frac{5}{48}} \sin \chi \cos \theta - \frac{\cos \chi}{4} \\ h_5 &= -\sqrt{\frac{5}{6}} \sin \chi \sin \theta \sin \left( \phi + \frac{\pi}{6} \right) \\ &\quad - \sqrt{\frac{5}{48}} \sin \chi \cos \theta - \frac{\cos \chi}{4}. \end{aligned}$$

The geometry of this model can be visualised by considering a slice through it. To this end, consider the surface  $\chi = \chi_0$  for  $\chi_0 = \cos^{-1}(-1/4) \approx 1.82$ . Its metric is given by

$$dl^2 = \frac{15}{16} \psi^4(\chi_0, \theta, \phi) d\Omega^2 \quad (19)$$

To get a rough idea of the shape of this hypersurface we can think of  $\theta$  and  $\phi$  as polar angles in  $E^3$  and plot the surface  $\psi(\chi_0, \theta, \phi) = \rho$  where  $\rho^2 = x^2 + y^2 + z^2$ . This surface is displayed in Fig. 1a and goes through 4 of the 5 masses. It should be noted that the surface does

not represent an isometric embedding of the geometry in Eq. (19). However, in regions where the derivatives of  $\psi$  are small, it does give an approximate representation of that geometry. This approximation is therefore best in regions which are far from the sources.

Point	$(w, x, y, z)$	$(\chi, \theta, \phi)$
(i)	$(1, 0, 0, 0)$	$(0, \frac{\pi}{2}, \frac{\pi}{2})$
(ii)	$(-\frac{1}{4}, \frac{\sqrt{15}}{4}, 0, 0)$	$(\cos^{-1}(-\frac{1}{4}), 0, \frac{\pi}{2})$
(iii)	$(-\frac{1}{4}, -\sqrt{\frac{5}{48}}, \sqrt{\frac{5}{6}}, 0)$	$(\cos^{-1}(-\frac{1}{4}), \cos^{-1}(-\frac{1}{3}), 0)$
(iv)	$(-\frac{1}{4}, -\sqrt{\frac{5}{48}}, -\sqrt{\frac{5}{24}}, \sqrt{\frac{5}{8}})$	$(\cos^{-1}(-\frac{1}{4}), \cos^{-1}(-\frac{1}{3}), \frac{2\pi}{3})$
(v)	$(-\frac{1}{4}, -\sqrt{\frac{5}{48}}, -\sqrt{\frac{5}{24}}, -\sqrt{\frac{5}{8}})$	$(\cos^{-1}(-\frac{1}{4}), \cos^{-1}(-\frac{1}{3}), \frac{4\pi}{3})$

Table II: Coordinates  $(w, x, y, z)$  of the 5 masses in the embedding space  $E^4$ , as well as  $(\chi, \theta, \phi)$  on the background 3-sphere. In this table, and throughout,  $\cos^{-1}$  refers to the inverse cosine, and not its reciprocal.

### C. The 8-Cell model

We now proceed in a similar manner to find the geometry of the 8-cell (or *tesseract*) model. In this case the primitive cell of our lattice is a cube. To find the position of the centre of each cell we can again embed the structure in  $E^4$ , together with a unit 3-sphere. Alternatively, the positions of the masses can be found using the dual lattice, which in this case is the 16-cell. The positions of the masses are then given as in Table III.

The  $f_i$  from Eq. (14) are then found to be

$$\begin{aligned} f_1 &= \sin \left[ \frac{\chi}{2} \right] \\ f_2 &= \cos \left[ \frac{\chi}{2} \right] \\ f_3 &= \sin \left[ \frac{1}{2} \cos^{-1}(\cos \theta \sin \chi) \right] \\ f_4 &= \cos \left[ \frac{1}{2} \cos^{-1}(\cos \theta \sin \chi) \right] \\ f_5 &= \sin \left[ \frac{1}{2} \cos^{-1}(\cos \phi \sin \theta \sin \chi) \right] \\ f_6 &= \cos \left[ \frac{1}{2} \cos^{-1}(\cos \phi \sin \theta \sin \chi) \right] \\ f_7 &= \sin \left[ \frac{1}{2} \cos^{-1}(\sin \phi \sin \theta \sin \chi) \right] \\ f_8 &= \cos \left[ \frac{1}{2} \cos^{-1}(\sin \phi \sin \theta \sin \chi) \right]. \end{aligned}$$

The first two of these functions are identical to those corresponding to the 2-cell model, considered above.

We can again visualise the geometry of this model by considering a slice through it. In Fig. 1b we show the surface with  $\chi = \pi/2$ , which passes through 6 of the 8

<sup>6</sup> Dual lattices have the vertices and centres of each cell transposed with each other.

masses. The radial position of the surface at any given  $(\theta, \phi)$  is proportional to  $\psi$ .

Point	$(w, x, y, z)$	$(\chi, \theta, \phi)$
(i)	(1, 0, 0, 0)	$(0, \frac{\pi}{2}, \frac{\pi}{2})$
(ii)	(-1, 0, 0, 0)	$(\pi, \frac{\pi}{2}, \frac{\pi}{2})$
(iii)	(0, 1, 0, 0)	$(\frac{\pi}{2}, 0, \frac{\pi}{2})$
(iv)	(0, -1, 0, 0)	$(\frac{3\pi}{2}, \pi, \frac{\pi}{2})$
(v)	(0, 0, 1, 0)	$(\frac{\pi}{2}, \frac{\pi}{2}, 0)$
(vi)	(0, 0, -1, 0)	$(\frac{3\pi}{2}, \frac{\pi}{2}, \pi)$
(vii)	(0, 0, 0, 1)	$(\frac{\pi}{2}, \frac{\pi}{2}, \frac{\pi}{2})$
(viii)	(0, 0, 0, -1)	$(\frac{3\pi}{2}, \frac{\pi}{2}, \frac{3\pi}{2})$

Table III: Coordinates  $(w, x, y, z)$  of the 8 masses in the embedding space  $E^4$ , as well as  $(\chi, \theta, \phi)$  in the lattice.

#### D. Models with 16-600 Equally Spaced Masses

We can construct the other discrete models, made using 16, 24, 120 and 600 equally spaced masses, by proceeding in a similar way to the cases discussed in detail above. We shall not present the details of these constructions here, but to help with their visualisation we display slices through these structures in Figures 1c-1f. It can be seen that as the number of masses increases, the shape of each of these structures becomes increasingly spherical, while the tubes become thinner. This corresponds to the spacetime approaching homogeneity as the number of masses is increased. We will use the results obtained from studying these larger lattice models in the sections that follow.

#### V. LOCATION OF THE HORIZONS

To qualify as cosmological solutions we require that the discrete models considered here avoid having any overlap in the horizons corresponding to different masses. We therefore need to investigate the positions of the horizons in the models discussed in the previous section, in order to see if this criterion is met. In these models the location of the event horizon can be approximated by marginally trapped surfaces [26] (such surfaces give the exact locations of the event horizons if the spacetime is static).

To find these trapped surfaces let us consider a surface given by some function  $\chi = \chi(\theta, \phi)$ . This surface has geometry

$$d\sigma^2 = \psi^4(\chi_{,\theta}^2 + \sin^2\chi)d\theta^2 + 2\chi_{,\theta}\chi_{,\phi}\psi^4d\theta d\phi + \psi^4(\chi_{,\phi}^2 + \sin^2\chi\sin^2\theta)d\phi^2,$$

and the unit normal to it is

$$n_\mu = \frac{\psi^2 \sin \chi \sin \theta}{\sqrt{\sin^2 \chi \sin^2 \theta + \sin^2 \theta \chi_{,\theta}^2 + \chi_{,\phi}^2}} (1, -\chi_{,\theta}, -\chi_{,\phi}^2),$$

where commas in subscripts denote partial differentiation. The extrinsic curvature of this surface is then  $K_{\mu\nu} = n_{\mu;\nu}$ , where the covariant derivative here is with respect to the metric of the 3-space. Transforming to coordinates  $a, b, \dots$  on the 2-space, using  $K_{ab} = \frac{\partial x^\mu}{\partial x^a} \frac{\partial x^\nu}{\partial x^b} K_{\mu\nu}$ , the trapped surfaces are those that have  $K = \gamma^{ab} K_{ab} = 0$ , where  $\gamma^{ab}$  is the contravariant induced metric on the 2-space. This condition is satisfied if

$$\begin{aligned} & 4 \sin^2 \chi \sin \theta (1 + \chi_{|\phi}^2)(1 + \chi_{|\theta}^2) (\chi_{|\phi} \psi_{|\phi} + \chi_{|\theta} \psi_{|\theta} - \psi_{,\chi}) \\ & + \psi \sin \theta \left[ (1 + \chi_{|\phi}^2 + \chi_{|\theta}^2) \chi_{|\phi} \phi + (1 + \chi_{|\phi}^2) \chi_{|\theta} \theta \right] \\ & + \psi \cos \chi \sin \theta [(1 + \chi_{|\phi}^2) \chi_{|\theta}^2 + \chi_{|\phi}^2 (1 + \chi_{|\phi}^2 + \chi_{|\theta}^2) \sin \theta \\ & \quad - \sin \chi (2 + 3\chi_{|\phi}^2 + (3 + 4\chi_{|\phi}^2) \chi_{|\theta}^2)] \\ & = -\psi \sin \chi \cos \theta \chi_{|\theta} (1 + \chi_{|\theta}^2), \end{aligned} \quad (20)$$

where for compactness we have introduced the notation  $\chi_{|\theta} \equiv \frac{1}{\sin \chi} \chi_{,\theta}$ , and  $\chi_{|\phi} \equiv \frac{1}{\sin \chi \sin \theta} \chi_{,\phi}$ . The positions of the horizons are then approximated by the solution to this equation.

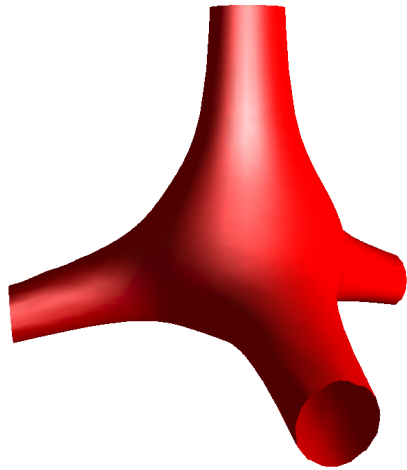
In practise Eq. (20) is not easy to solve, but we can obtain approximate solutions by looking for minimal surfaces of constant  $\chi$ , for which Eq. (20) reduces to  $(\psi^4 \sin^2 \chi)_{,\chi} = 0$ . We expect this to be a good approximation for all the models considered here, and for its accuracy to increase as the number of masses in the lattice is increased. To establish this result we calculate the area of the horizon of each mass using our approximation,  $A_{\min}$ , as well as the horizon area of a Schwarzschild black hole with an equal proper mass,  $A_S$ . We then calculate the ratio  $(A_{\min} - A_S)/A_S$ , which we have displayed in Table IV. As expected, the difference is small, and decreases as the number of masses is increased.

To check that the horizons are not overlapping we compare  $\chi_{\min}$  with half the separation between neighbouring sources,  $\Delta\chi$ . This is also displayed for each of our 6 discrete models in Table IV. It can be seen that  $\chi_{\min}$  is always less than half  $\Delta\chi$ , and that it decreases as the number of masses is increased. Together with the small values of  $(A_{\min} - A_S)/A_S$  this provides a good indication that the horizons of the masses in our models do not intersect at the maximum of expansion, thus ensuring that our discrete models satisfy a necessary condition to qualify as cosmological models<sup>7</sup>.

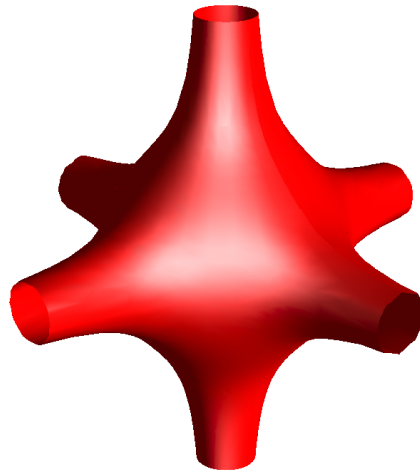
#### VI. BACKREACTION IN DUST MODELS

We shall now employ our exact discrete solutions in order to study backreaction in dust-filled cosmological

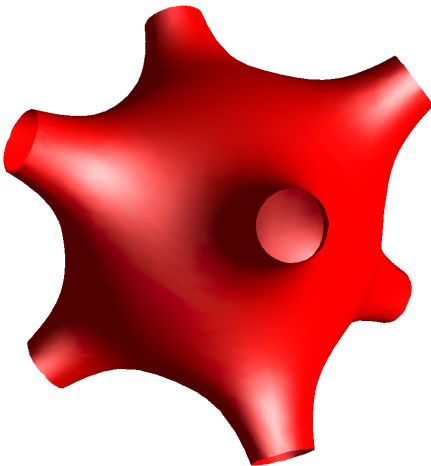
<sup>7</sup> We leave aside for now the more complicated question of whether there are additional horizons that could encompass two or more masses. We note only that this would appear to be unlikely, given that in every case the masses are separated by multiple horizon distances.



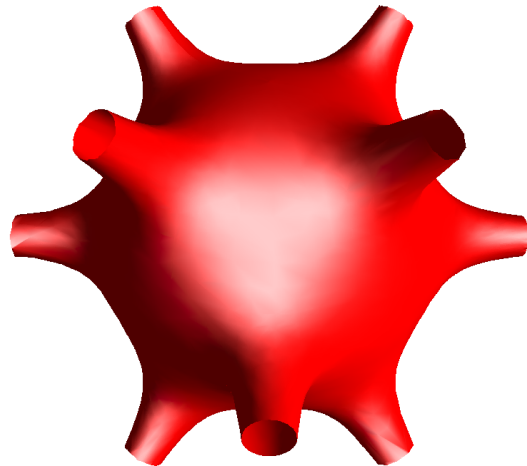
(a) A slice through the 5-cell solution



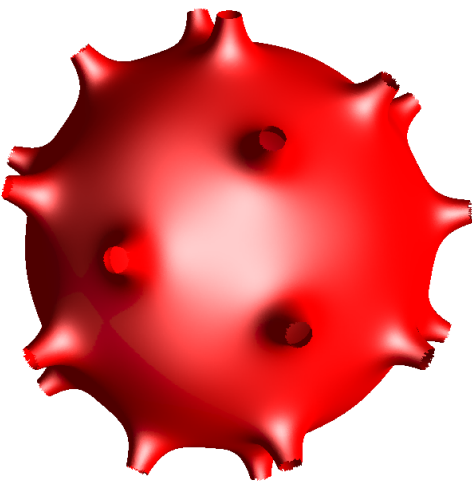
(b) A slice through the 8-cell solution



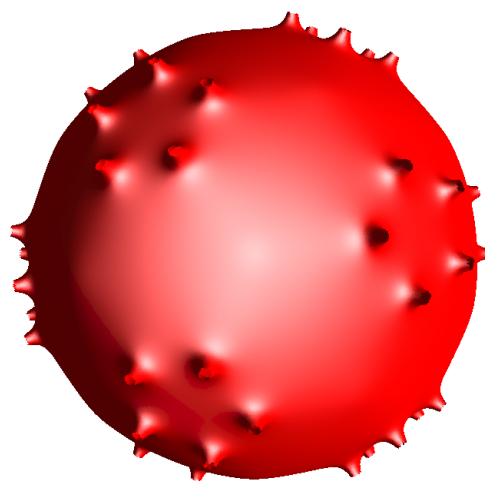
(c) A slice through the 16-cell solution



(d) A slice through the 24-cell solution



(e) A slice through the 120-cell solution



(f) A slice through the 600-cell solution

Figure 1: Slices through the hypersurfaces of the discrete lattice solutions. The distance from the centre is proportional to  $\psi$ . The tubes correspond to the locations of the masses. These objects become more and more spherical as the number of sources in the lattice increases.



Number of Masses	$\frac{A_{\min} - A_S}{A_S}$	$\frac{\chi_{\min}}{\Delta\chi/2}$
5	$1.55 \times 10^{-6}$	0.428
8	$7.15 \times 10^{-9}$	0.268
16	$3.46 \times 10^{-9}$	0.173
24	$9.95 \times 10^{-13}$	0.110
120	–	0.0330
600	–	0.0147

Table IV: The fractional difference between our estimate of the horizon size,  $A_{\min}$ , and the horizon size of a Schwarzschild black hole with the same proper mass,  $A_S$ . Also displayed is our estimate of the fraction of the distance to the point half-way between masses that the horizon reaches, for each of our discrete models. Dashes indicate numbers smaller than our numerical precision.

models. This will be done by comparing the scale of discrete and continuous models on their time-symmetric hypersurfaces, at the maximum of expansion.

Here we will make use of the notion of ‘proper mass’ in order to compare our lattice models with the dust-filled ( $k = +1$ ) FLRW solutions. That is, for a given lattice we will calculate the total proper mass of all the sources in the lattice, and we will then compare this lattice to an FLRW solution with the same total proper mass. The motivation for this procedure is that in both cases, the proper mass corresponds to locally measured masses. Specifically, for the FLRW models, the proper mass for a given region can be defined as the integral of the energy density over that region. For the lattice models, the mass within each cell is identified with the proper mass of the source it contains, so that the total proper mass of the lattice is given by the sum of the proper masses of all the sources within it.

The geometry of the time-symmetric hypersurface of maximum expansion in ( $k = +1$ ) FLRW solutions is now given by Eq. (5). On the other hand, the metric corresponding to the 3-sphere containing  $n$  discrete masses of equal size is given by Eq. (14), with  $\tilde{m}_{i+1} = \tilde{m}_i$  for every  $i < n$ . The value of  $\tilde{m}_i$  can then be related to the proper mass of each of the objects using the procedure outlined in Section III B. In order to compare continuous and discrete solutions we then only need to make sure that the mass of the continuous solutions (defined as the constant  $M = \rho V$  where  $V$  is the total spatial volume of the universe) is the same as the sum of the proper masses in the discrete solutions.

In the discrete solutions, consisting of  $n$  objects each with proper mass  $m$ , the total mass is clearly just  $M = nm$ . In the FLRW solutions the volume of a spatial section of constant  $t$  is given by  $V = 2\pi^2 a^3$ , where  $a = a(t)$  is the scale factor. Thus the energy density for a ( $k = +1$ ) FLRW solution with the same total mass ( $M$ ) is given at its maximum of expansion by

$$\rho(t_0) = \frac{M}{V} = \frac{M}{2\pi^2 a^3(t_0)}. \quad (21)$$

Recalling that in a ( $k = +1$ ) FLRW solution the maximum of expansion occurs when  $a^2 = 3/(8\pi\rho)$ , the line-element (5) can be written as

$$dl^2 = \frac{16M^2}{9\pi^2} (d\chi^2 + \sin^2\chi d\theta^2 + \sin^2\chi \sin^2\theta d\phi^2). \quad (22)$$

We can now compare this geometry with the corresponding discrete geometry given by Eq. (14).

To proceed we require a measure of the global scale for both the discrete and the continuous solutions. In the continuous case it is clear what this measure should be, as there is only one scale in the geometry (the curvature of the 3-sphere). For the discrete solutions, on the other hand, the length of a curve of fixed angle on the 3-sphere will depend on its particular position, as the geometry of the space is inhomogeneous in these solutions. We must therefore proceed with some care. Here, for the discrete solutions, we propose two possible measures of the ‘size’ of the space. These are:

- D1 The line-element,  $dl$ , of a curve at a vertex of the lattice. These are clearly distinguished positions within the lattice, corresponding to the points that are furthest from all masses.
- D2 The length of the edge of a cell. Again, this is clearly a preferred curve within the lattice.

Both of these proposed definitions of size are aimed at trying to identify the scale of the lattice structure that the masses occupy, as this is the closest thing to a ‘background’ that exists in these solutions. Identifying the size of the lattice was also what was attempted by Lindquist and Wheeler in their approximate solution with the same configuration of masses [17]. Within this context, Definition D1 will turn out to be the most conservative possible comparison of the scales of the discrete and continuous solutions, and Definition D2 will be found to be not very different.

Let us first consider Definition D1. In this case it can be seen that the ratio of the line-elements of curves that cover the same angle on the 3-sphere in the continuous and the discrete solutions is given by

$$\frac{dl^{\text{discrete}}}{dl^{\text{FLRW}}} = \frac{3\pi\tilde{m}_i}{16nm} \left( \sum_{i=1}^n f_i^{-1} \right)^2. \quad (23)$$

Due to the fact that  $\tilde{m}_i$  can be shown to be in direct proportion to  $m$ , it can be seen that this expression is, in fact, independent of  $m$ . It is therefore specified uniquely by the structure of the lattice (i.e. by  $n$ , and the functions  $f_i$  corresponding to the lattice in question).

The ratio of scales in Eq. (23) is a function of  $\chi$ ,  $\theta$  and  $\phi$ , and so varies depending on which point in the discrete solution we wish to consider. Using Definitions D1 and D2, we find the results displayed in the third and fourth columns of Table V, respectively. Here  $a_0^{\text{discrete}}$  refers to the scale of discrete solution, as defined using D1 or D2. These results are also displayed graphically in Fig. 2,

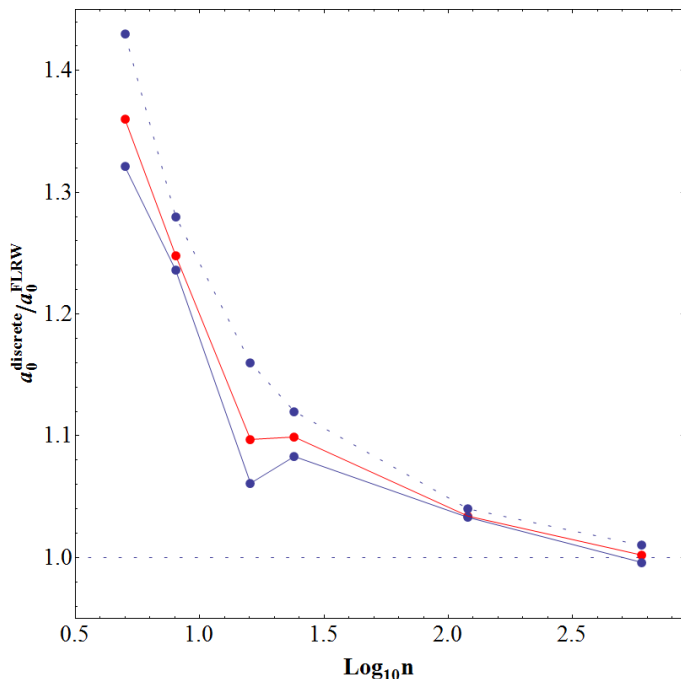


Figure 2: The scale of the discrete solutions as a fraction of the scale of the continuous solutions, when the total mass in the continuous model is taken to be equal to the total proper mass of the discrete model. The full blue curve shows the result of using Definition D1 for the scale of the discrete solution, and the red curve shows the result for Definition D2. The dotted blue curve which represents the approximate Lindquist-Wheeler solution is shown for comparison.

for each of our lattices. It can be seen that the scales corresponding to the discrete solutions is always larger than that of the corresponding continuous solution, with the only exception being the scale of the solution with 600 masses, when Definition D1 is used.

Figure 2 shows that  $a_0^{\text{discrete}}/a_0^{\text{FLRW}}$  approaches 1 as  $n$  becomes large, but that this approach is not exactly monotonic. In particular, the ratio for the lattice with 16 masses is a little lower than might have been the case for a smooth curve. This behaviour is likely to be a con-

Cell Shape	Number of Masses	$\left(\frac{a_0^{\text{discrete}}}{a_0^{\text{FLRW}}}\right)_{\text{D1}}$	$\left(\frac{a_0^{\text{discrete}}}{a_0^{\text{FLRW}}}\right)_{\text{D2}}$
Tetrahedron	5	1.321	1.360
Cube	8	1.236	1.248
Tetrahedron	16	1.061	1.097
Octahedron	24	1.083	1.099
Dodecahedron	120	1.033	1.034
Tetrahedron	600	0.996	1.002

Table V: The scale of the discrete solutions as a fraction of the scale of the continuous solutions, when the total mass in the continuous model is taken to be equal to the total proper mass of the discrete model. The two definitions of scale in the discrete solutions have both been calculated.

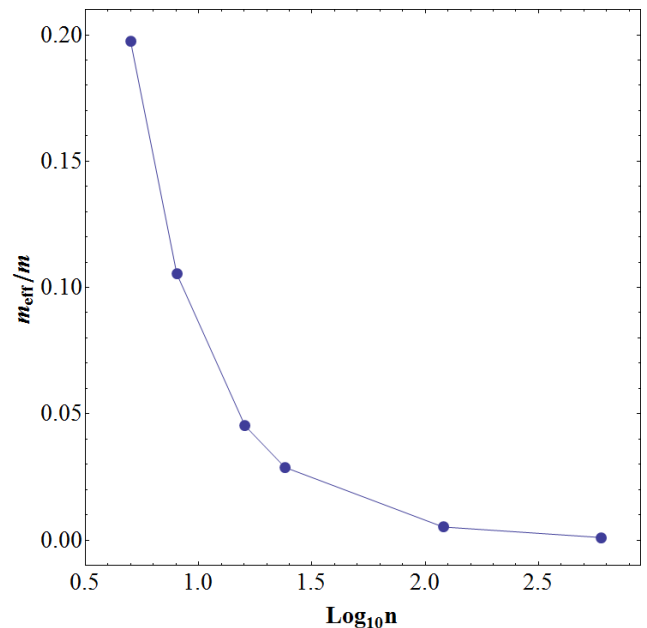


Figure 3: The ratio of the effective mass,  $m_{\text{eff}}$ , to the proper mass,  $m$ , for each lattice solution.

sequence of the fact that the shape of the cells used in different tessellations are different. For the lattice solutions made from tetrahedra (i.e. those with  $n = 5, 16, 600$  masses), for example, the approach to the FLRW limit does appear to be monotonic. For the sake of comparison, we have also shown in Fig. 2 the ratios obtained using the approximate solutions of Lindquist and Wheeler [17]. It can be seen that the ratios given by the approximate solutions compare well with those of the exact solutions.

The outcome of this comparison demonstrates that, for large numbers of regularly arranged masses at their maximum of expansion, this measure of backreaction in dust-filled models is small.

## VII. EFFECTIVE MASSES AND INTERACTION ENERGY

An advantage of the discrete models we consider is that they provide us with a framework within which it is possible to discuss the role of inter-particle interactions in cosmology. Given that these are the interactions that govern the structure and evolution of the real universe, we consider it to be an important undertaking to obtain a deeper understanding of them. In particular, interactions are ignored when approximating the universe as being filled with dust, and so these considerations potentially allows us further insights into the behaviour of spacetimes filled with discrete objects.

Here we will begin by comparing the notions of *proper mass* and *effective mass* for each of our discrete solutions, as defined in Section III B. We remind the reader that our definition of effective mass is based on analogy with the

Cell Shape	Number of Masses	$\frac{m_{\text{eff}}}{m}$
Tetrahedron	5	0.20
Cube	8	0.11
Tetrahedron	16	0.045
Octahedron	24	0.029
Dodecahedron	120	0.0052
Tetrahedron	600	0.0010

Table VI: The ratio of the effective mass,  $m_{\text{eff}}$ , to the proper mass,  $m$ , for each lattice.

asymptotically flat case studied by Brill and Lindquist [25], as it is problematic to define it operationally in the closed spherical settings we are currently studying. Now, the values of these masses can be set to any given value for each lattice, but the ratio of effective mass to proper mass must take a particular constant value for any given configuration. We display this ratio for each of the six possible tessellations in Table VI, and show it graphically in Fig. 3. It is clear that the ratio of effective mass to proper mass increases as the number of masses in the lattice is decreased. This is due to decreasing contributions from the interaction energies between particles, which correspondingly increase the value of the effective mass of each source.

In Fig. 4 we compare the scale of the hypersurface of maximum expansion for each of our discrete solutions, when the total effective mass of the lattice is kept constant. As the effective mass includes the inter-particle interaction energies, this procedure of comparing the scale of solutions with the same total effective mass is equivalent to enforcing the condition that the lattices being compared should contain the same total energy (that is, the same total proper mass plus interaction energies). Fig. 4 then shows that the scale of the hypersurface of maximum expansion grows approximately linearly with the number of masses,  $n$ . Changing the method of determining the scale of the discrete solutions from D1 to D2 has very little effect.

The results in Fig. 4 can be understood by considering Fig. 3 – as the number of masses decreases the ratio of the magnitude of interaction energies to proper mass also decreases. The interaction energies, however, are negative, so if we consider a thought experiment in which we deform the 8-cell into the 5-cell we have to *increase* the total amount of energy available for interactions. The only source of energy in the solution is the proper mass of the particles, and so a lattice with fewer masses must have a smaller total proper mass if the total energy in the system is to remain unchanged. Smaller total proper mass corresponds to a smaller scale for the hypersurface of maximum expansion, as was shown in Section VI. This result suggests that one can substantially increase the scale of a closed space by dividing up the mass in that space into smaller packets, although we have strictly only

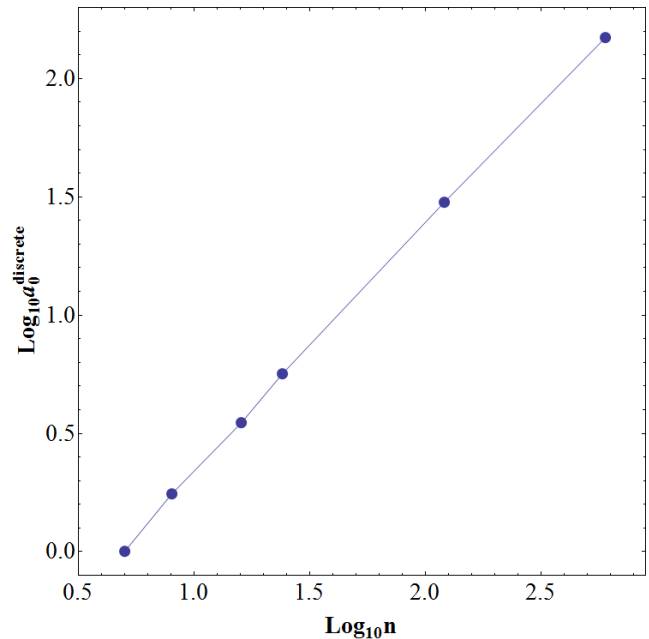


Figure 4: The scale of lattice solutions with the same total effective mass, normalised so that  $a_0 = 1$  for the 5-cell, and using D1 for the scale of the discrete solutions.

shown this is the case on time-symmetric hypersurfaces<sup>8</sup> It should also be noted that this result relies on the definition of effective mass that we have generalized from the asymptotically flat setting in order to define the interaction energies. The validity of this approach is difficult to confirm operationally in a compact space, and so the interpretation of the dramatic increases in scale seen here should be treated with care.

Such increases in scale are entirely absent in dust models, as interaction energies are not included in the energy budget in that case. This does not, however, invalidate any of the conclusions of Section VI. It remains the case that back-reaction is small in models where interaction energies are ignored. What has changed for the lattices in Fig. 4 is that the proper mass in each lattice is increasing as the number of masses is increased, so the dust-dominated FLRW solution that one should compare with these models is also changed.

## VIII. CONCLUSIONS

We have studied the emergence of spatially closed Friedmann solutions from inhomogeneous solutions that contain increasing numbers of regularly arranged discrete masses in topological 3-spheres. This has been done using

<sup>8</sup> For a dynamical cosmological model we no longer necessarily have energy conservation, and so the situation could be more complicated.

exact methods, and therefore allows for exact measures of backreaction in dust dominated cosmological models.

More specifically, by considering the instantaneously static hypersurfaces at the moment of maximum expansion we have found that universes that contain only a small number of mass concentrations ( $\lesssim 10$ ) can be 10% or more larger than the corresponding dust dominated FLRW solutions of Einstein's equations. However, for universes that contain very many masses ( $\gtrsim 100$ ) there is very little quantitative difference ( $\lesssim 1\%$ ) between the scale of maximum of expansion in the discrete and continuous solutions. These results are based on comparing dust dominated continuous models (which ignore the inter-particle interaction energies) with momentarily static discrete models that contain the same total 'proper mass' (which also ignores the interaction energies between the different masses). While backreaction in this case is quite small, it may well be that the inter-particle interactions will come into play in a more substantive way when we allow for dynamics. That is, backreaction could still have a big effect when we consider the evolution of the universe.

The results we find are in good keeping with the approximate solutions of Lindquist and Wheeler that use a gravitational analogue of the Wigner-Seitz construction [17], as is demonstrated graphically in Fig. 2. They also present us with exact expressions for the change in scale of cosmological solutions that has been predicted using Zalaletdinov's averaging scheme [32–34]. More generally, we believe our study could allow some insight into the problem of how averaging should be performed in relativistic cosmology. To date, most studies on this subject have used either highly symmetric exact solutions that contain a perfect fluid, or have considered small fluctuations around an FLRW "background" geometry. The former approach is strongly limited by the high degree of symmetry required in the solutions, while the latter is limited to geometries that are already necessarily close to FLRW. The models we have constructed here suffer from neither of these shortcomings, as they admit no Killing vectors, and do not require the assumption of an FLRW geometry, either as a boundary condition for the inhomogeneities, or as a background geometry. As such it offers a new laboratory for testing ideas about inhomogeneity, averaging, and backreaction in cosmology.

With the notion of effective mass employed here, we find the interaction energy grows rapidly as the number of masses in the lattice, and comes to dominate in the limit of very many masses. This means that if we compare lattices with different numbers of masses, but with the same total energy (including interaction energy), then the scale of the hypersurface of maximum expansion increases dramatically with increasing number of masses. As was discussed above, however, the interpretation of this effect requires some care, as it is based on a generalization of the definition of effective mass given by Brill and Lindquist in asymptotically flat settings. Nevertheless, this effect is entirely neglected when treating the matter content of the universe as dust.

Finally, in this paper, we have confined ourselves to the comparison of the discrete and continuous models on time symmetric hypersurfaces. Clearly the next step would be to make a detailed comparison of the full evolution of these models. We shall return to this question in future publications. We also note that, although we have only considered regular arrangements of masses in this paper, the formalism we have used allows for the possibility of considering much more complicated distributions.

**Note added.** After submission of our manuscript the following related work appeared: [35–37]. The first of these papers performs a numerical analysis of a spatially flat lattice of black holes [35], while the second performs a perturbative analysis of a similar situation [36]. The third study finds exact initial data for a lattice of eight black holes in a space with spherical topology (using the same method presented in this paper), and then proceeds to numerically evolve this data [37].

#### Acknowledgements.

TC acknowledges the support of the STFC and the BIPAC. TC and RT thank the hospitality of UCT for a visit in February 2011, and TC and KR thank the AU, QMUL for a visit in October 2011. We are grateful to George Ellis, Helena Engström, Pedro G. Ferreira, Daniele Gregoris, Roy Maartens and Bruno Mota for helpful comments and discussions.

- 
- [1] Ellis, G. F. R., *General Relativity and Gravitation*, R. Reidel Publishing Co., Dordrecht, ed. Bertotti, B, de Felice F. & Pascolini, A., pp.215-288 (1984).
  - [2] Räsänen, S., *JCAP* **02**, 011 (2009).
  - [3] Räsänen, S., *JCAP* **03**, 018 (2010).
  - [4] Bull, P. & Clifton, T., *Phys. Rev. D* **85**, 103512 (2012).
  - [5] Buchert, T. & Räsänen, S., *Ann. Rev. Nucl. Part. Sci.* **62**, 57 (2012).
  - [6] Clarkson, C., Ellis, G. F. R., Larena, J. & Umeh, O., *Rept. Prog. Phys.* **74**, 112901 (2011).
  - [7] Komatsu, E. *et al.*, *Astrophys. J. Suppl.* **192**, 18 (2011).
  - [8] Keisler, R. *et al.*, *Astrophys. J.* **743**, 28 (2011).
  - [9] Guy, J. *et al.*, *Astron. & Astrophys.* **523**, A7 (2010).
  - [10] Kessler, R. *et al.*, *Astrophys. J. Suppl.* **185**, 32 (2009).
  - [11] Eisenstein, D. J. *et al.*, *Astrophys. J.* **633**, 560 (2005).
  - [12] Cole, S. *et al.*, *MNRAS* **362**, 505 (2005).
  - [13] Bridle, S. L., Lahav, O., Ostriker, J. P., & Steinhardt, P. J., *Science* **299**, 1532 (2003).
  - [14] Wiltshire, D. L., *Class. Quant. Grav.* **28**, 164006 (2011).
  - [15] Bertotti, B., *Proc. Roy. Soc. Lond. A* **294**, 195 (1966).

- [16] Rosquist, K., “Aspects of the Discrete Universe” in *Proceedings of the XIV Brazilian School of Cosmology and Gravitation*, Cambridge Scientific Publishers, 2012 (in press).
- [17] Lindquist, R. W. & Wheeler, J. A., *Rev. Mod. Phys.* **29**, 432 (1957); *erratum*, *Rev. Mod. Phys.* **31**, 839 (1959).
- [18] Clifton, T. & Ferreira, P. G. *Phys. Rev. D* **80**, 103503 (2009); *erratum*, *Phys. Rev. D* **84**, 109902 (2011).
- [19] Clifton, T. & Ferreira, P. G., *JCAP* **10**, 26 (2009).
- [20] Clifton, T., Ferreira, P. G. & O’Donnell, K., *Phys. Rev. D* **85**, 023502 (2012).
- [21] O’Donnell, K., *Optical Properties of the Lindquist-Wheeler Cosmology*, Honours project, University of Canterbury, New Zealand (2011).
- [22] Clifton, T., *Class. Quant. Grav.* **28**, 164011 (2011).
- [23] Collins, P.A. & Williams, R. M., *Phys. Rev. D* **7**, 965 (1973).
- [24] Misner, C. W. *Ann. Phys.* **24**, 102 (1963).
- [25] Brill, D. R. & Lindquist, R. W., *Phys. Rev.* **131**, 471 (1963).
- [26] Gibbons, G. W., *Commun. Math. Phys.* **27**, 87 (1972).
- [27] Cadez, A., *Ann. Phys.* **83**, 449 (1974).
- [28] Korotkin, D., and Nicolai, H., arXiv:gr-qc/9403029 (1994).
- [29] Wald, R. M., p.126 of *General Relativity*, The University of Chicago Press, Chicago (1984).
- [30] Coxeter, H. M. S., *Regular Polytopes*, Methuen and Company Ltd., London (1948).
- [31] Uzan, J.-P., Ellis, G. F. R. & Larena, J., *Gen. Rel. Grav.* **43**, 191 (2011).
- [32] Coley, A. A., Pelavas, N. & Zalaletdinov, R. M., *Phys. Rev. Lett.* **95**, 151102 (2005).
- [33] van den Hoogen, R. J., *J. Math. Phys.* **50**, 082503 (2009).
- [34] Zalaletdinov, R. M., *Bull. Astron. Soc. India* **25**, 401 (1997).
- [35] Yoo, C.-M., Abe, H., Takamori, Y. & Nakao, K.-I., *Phys. Rev. D* **86**, 044027 (2012).
- [36] Bruneton, J.-P. & Larena, J., *Class. Quant. Grav.* **29**, 155001 (2012).
- [37] Bentivegna, E. & Korzynski, M., *Class. Quant. Grav.* **29**, 165007 (2012).